IEEE Access
Multidisciplinary | Rapid Review | Open Access Journal

Received 27 May 2024, accepted 20 June 2024, date of publication 1 July 2024, date of current version 16 July 2024.

Digital Object Identifier 10.1109/ACCESS.2024.3421279

RESEARCH ARTICLE

Diagnosis of Osteoporosis by Bone X-Ray Based on Non-Destructive Compression

CHAO JIANG, YUQI CHENG, AND BAOSHENG CHENG
Changshan County Hospital of Traditional Chinese Medicine, Quzhou 324200, China
Corresponding author: Yuqi Cheng (cyq19740330@163.com)

ABSTRACT X-ray is a commonly used imaging method for the diagnosis and evaluation of osteoporosis, which has crucial clinical diagnostic significance. To ensure the high fidelity requirements of medical image diagnosis and achieve high-quality transmission and storage of image data, this study uses deep learning to design a dual stream lossless compression network suitable for X-ray images. The results demonstrated that the designed network performed well in compression and bit rates on different datasets, with a minimum bit rate of 0.204 and a maximum compression rate of 0.946. Compared to other advanced models, this network had the highest peak signal-to-noise ratio and lower distortion of compressed images. In the compression process of X-ray images of osteoporosis, this network outperformed other models in different structural similarity indices, with values above 0.90, showing significant advantages. The equivalent number of views of the compressed image reached 0.93, and the visual quality of the lossless compressed image was high, ensuring the efficiency and accuracy of diagnosis. The research method can significantly improve the theoretical research level of lossless compression technology and enhance its practical value in remote medical diagnosis.

INDEX TERMS Lossless compression, medical imaging, neural network, osteoporosis, X-ray.

I. INTRODUCTION

Osteoporosis is often characterized by a decrease in bone tissue quality and density, and fragile bones that are prone to fractures. It is a skeletal system disease caused by age, genetic factors, unhealthy lifestyle habits, or other diseases and medications. Digital X-ray is an important diagnostic method for assessing bone tissue quality and distinguishing the presence of osteoporosis [1], [2]. With the advancement of medical imaging instruments and medical technology, the use of digital X-ray imaging (DX-rayI) to diagnose osteoporosis has become a common treatment method, generating a considerable amount of image data in medical institutions. Therefore, storing and retrieving a large number of X-ray images has become a problem faced by medical organizational structures. At the same time, telemedicine is gradually emerging, and sending and transmitting high-quality medical imaging data is crucial for ensuring accurate and reliable medical diagnosis. However, there are differences in the services and equipment of various medical institutions, and using DX-rayI to achieve remote diagnosis of osteoporosis still poses challenges [3]. With the surge in the amount of imaging data and the demand for remote medical care, the use of computer vision technology to assist radiologists in clinical diagnosis has become an important research trend in order to effectively process, collect, and transmit medical images [4]. Image compression is an image signal processing technique that saves data storage space and transmission bandwidth by reducing the size of image files to accelerate transmission speed. Common image compression methods include lossy compression and lossless compression. Lossy compression requires sacrificing some image quality, which can easily cause loss of image details and artifacts, and does not meet the diagnostic requirements of medical images. Lossless compression can balance the need to reduce file size and preserve image

The associate editor coordinating the review of this manuscript and approving it for publication was Carmelo Militello.

details as much as possible. However, currently, lossless compression techniques are mostly aimed at natural images with low dynamic range (LDR), while DX-rayI used for the diagnosis of osteoporosis belongs to high dynamic range (HDR) images. The existing lossless compression technology cannot be directly applied to the diagnosis of osteoporosis DX-rayI [5]. Therefore, in order to ensure the high fidelity requirements of medical diagnosis, this study innovatively abandons traditional encoder decoder structures and chooses deep learning (DL) technology, utilizing end-to-end advantages to simultaneously compress high and low sub images, and designs a dual stream image compression network for HDR images. This study is expected to improve the efficiency of medical personnel in processing and analyzing medical imaging data, and enhance the diagnostic efficiency and accuracy of osteoporosis.

The research content mainly consists of four parts. Part 1 mainly elaborates on the research status and progress of image lossless compression technology in medical and other fields, and outlines the shortcomings of the research. Part 2 designs a dual stream lossless compression network (DSLC-Net) based on feature fusion. Part 3 conducts performance testing and application analysis on lossless compression algorithms. Part 4 summarizes the experimental results.

II. LITERATURE REVIEW

The rise of image compression technology provides efficient technical support for managing and storing large amounts of data. In order to further improve the compression ratio (CR) and image fidelity of compression technology, domestic and foreign scholars have conducted a series of studies on the optimization and improvement of compression technology. Remote healthcare enables the exchange of medical diagnostic data based on the Internet of Things, but the massive amount of medical information results in the actual cost of transmitting medical data with limited bandwidth being too high. To ensure the compression quality of medical images, Mohammadi et al. [6] designed a hybrid medical information compression technique that combines Huffman encoding and rearrangement information. This method utilized binary information arrangement to ensure the compression quality and efficiency of the technology, and the restored image quality was relatively high. Residual encoding has been widely used in lossless compression. Liu et al. [7] used video codecs as lossy layers and networks based on bilateral context modeling as residual layers to design a 3D medical image residual encoding framework for lossless compression. This method could effectively reduce redundant information and had better performance than existing advanced models. The non-integer reversible nature of traditional discrete shmaliy moment transform (DST) was not suitable for lossless image applications. To overcome technical limitations, Daoui et al. [8] introduced integer DST and proposed a one-dimensional chaotic system model, which was applied to reversible image processing. Medical image compression experiments have shown that this method has a good CR and can achieve safer medical image transmission.

3D radiological images are crucial in radiology. To meet the high compression requirements for storage and transmission of 3D radiographic images, Boopathiraja et al. [9] used optimal multilinear singular value decomposition to solve the volume of interest in the image. It also used an adaptive binary range encoder for image compression, and finally decompressed to reconstruct the original image. This method had a good compression rate of up to 37.31 and the lowest bit rate (BR) of 0.21. Repeated magnetic resonance imaging scans generated massive amounts of image data. To reduce memory requirements, Jumakulyyev and Schultz [10] designed a new lossless nuclear magnetic resonance diffusion data codec. This method introduced q-space partial differential equations, and the compression rate was effectively improved. To improve the attention of the deep generative model PixelCNN to important information at long distances, Jiang et al. [11] combined causal attention modules with residual connections and used mixed residual causal attention modules to improve the performance of PixelCNN. Verified by the HTRU1 dataset, this method improved the modeling ability of the model for pulsar data and enhanced its lossless compression ability. To achieve lossless compression of Tc-99 m radioactive nuclide renal static imaging (Dimercaptosuccinic acid), Yadav et al. [12] improved and optimized the coefficient threshold of discrete cosine transform (DCT). After verification by eight image quality indicators, the improved DCT lossless compression technology in this study achieved high-quality image compression without significant loss of clinical details. The optimal thresholds were 10, 15, and 20. The massive increase in image data has brought difficulties to the storage and transmission of images. To meet the high fidelity requirements and improve the lossless image CR, Liu et al. [13] designed an improved lossless image compression algorithm based on integer wavelet transform and Huffman coding. This method was superior to existing advanced algorithms, with a CR improvement of at least 6.22%, reaching 72.36%. The healthcare industry involved the storage and protection of a large amount of confidential information. Reddy et al. [14] designed an improved string table compression algorithm and completed information encryption protection based on symmetric/asymmetric key encryption. This method reduced the time required to generate keys by 1/4, encrypts data by 20%, and significantly saved resources on compressed image information.

In summary, there have been many studies and applications on lossless compression algorithms, but most of them use codecs as the core technology of lossless compression. This approach has poor adaptability to HDR images, and the compression quality and efficiency are difficult to meet the needs of medical image diagnosis. In this regard, this study conducted lossless compression research on HDR images based on DL technology.

III. DESIGN OF A LOSSLESS COMPRESSION MODEL FOR DUAL STREAM X-RAY IMAGES BASED ON END-TO-END DL

To store and transmit large-scale X-ray HDR image data and ensure high image fidelity, this study uses DL technology to design a lossless compression algorithm.

A. DESIGN OF HIGH 8-BIT DEEP SUB-GRAPH COMPRESSION NETWORK BASED ON LOSSY PLUS RESIDUAL

Common medical imaging techniques, such as computed tomography (CT) and X-ray, consist of multiple slice images. The pixel grayscale levels of different slice images can be represented as values between 2^{12}-2^{16}, meaning that the single channel depth of the image is 12-16 bit deep. High bit depth provides richer image information for clinical diagnosis, which helps to obtain more comprehensive information about the condition [15]. Traditional 2D codecs, multi-layer codecs, and lossless codecs are not suitable for lossless compression of HDR slice images [16]. In this study, a layer by layer lossless compression method is proposed to improve compression performance by dividing the bits of HDR slice images. This study takes a 16 bit deep X-ray image as an example, defined as X. The schematic diagram of the designed dual stream compression model structure is Figure 1.

In Figure 1, the first is to divide X into two sub-graphs, x^h and x^l. x^h and x^l represent images with high and low 8-bit depth. By designing a network to adjust the BR of different depth images, the total BR is minimized. There are significant differences between x^h and x^l in terms of information content such as resolution, CR, file size, and information richness. x^l has higher resolution and details, lower compression rate, larger file size, and more image details. Usually, x^l requires a higher BR, while x^h only accounts for 10% of the total BR. Therefore, the design of the x^h compression network should be as concise as possible, controlling the number of model parameters, and consisting of two parts: a lossy compression model and a residual compression model. The lossy compression model structure of the sub-graph module with a high 8-bit bit depth is Figure 2.

In Figure 2, the overall structure of the 8-bit deep image is a lossy compression network based on a hyper-priori model. The lossy compression framework can complete image reconstruction using an encoder and decoder, and the calculation process is equation (1).

$$\widehat{x} = \wp_s\left(y;\theta_s\right) = \wp_s\left(Q\left(\wp_a\left(x;\theta_a\right)\right);\theta_s\right) \tag{1}$$

In equation (1), $\wp_a$ and $\wp_s$ represent the encoder and decoder, respectively. $\widehat{x}$ and x represent reconstructed images and input images, respectively. Q represents the quantization function. θ represents the model parameters. y represents discretized encoding.

In the lossy compression model, after x^h is input into the network, the encoder converts it into a latent spatial representation y^h and performs downsampling operations to reduce the scale of the image, ensuring that y^h is compact in size and independent in content. Then, the hyperpriori encoder extracts edge information from y^h and uses the decoder to convert the edge information into the probability model parameters of y^h, thereby generating the hidden feature $\widehat{y}^h$ of y^h. At the same time, the decoder will generate lossy reconstructed image $\widehat{x}^h$ and reconstructed feature u^h. The decoder performs a reverse upsampling operation to restore the image scale. This process achieves high-quality image reconstruction by compressing and reconstructing important features, ensuring consistency in scale and content between the reconstructed image and the original image. The hidden features in the lossy compression model are modeled using a Gaussian model, and the estimated probability distribution of hidden feature $\widehat{y}^h$ is calculated using equation (2).

$$\begin{aligned} p_{\theta^h}\left(\widehat{y}^h\middle|\widehat{z}^h\right) &= \prod_i\left(\mathbb{N}\left(\mu_i,\sigma_i^2\right) * U\left(-\frac{1}{2},\frac{1}{2}\right)\right)\left(\widehat{y}^h,i\right), \\ \mu_i,\sigma_i^2 &= f_{hpd}\left(\widehat{z}^h\right) \end{aligned} \tag{2}$$

In equation (2), $p_{\theta^k}\left(\widehat{y}^h\middle|\widehat{z}^h\right)$ represents the estimated probability distribution. f_{hpd} is a Gaussian distribution. μ_i and σ_i^2 are the corresponding mean and variance. f_{hpd} represents a super prior decoder. $\widehat{z}^h$ represents the characteristics of edge information. i represents the spatial position of the index. The edge information adopts a decomposable entropy model and completes entropy encoding using $\widehat{z}^h$'s prior probability distribution. The calculation process of the BR $R_{\widehat{y}^h,\widehat{z}^h}$ for the lossy BR of x^h is equation (3).

$$\begin{aligned} R_{\widehat{y}^h,\widehat{z}^h} &= \mathrm{E}_{P(x^h)}\mathrm{E}_{q_\phi\left(\widehat{y}^h,\widehat{z}^h\middle|x^h\right)} \\ &\times\left[-\log p_\theta\left(\widehat{y}^h\middle|\widehat{z}^h\right)-\log p_\theta\left(\widehat{z}^h\right)\right] \end{aligned} \tag{3}$$

In equation (3), E represents the measure of mean square error. p represents the actual probability distribution. $q^{\left(\widehat{y}^h,\widehat{z}^h\middle|x^h\right)}$ represents the inference model. ϕ represents a parameter. The calculation of residual r^h in the residual compression model is equation (4).

$$r^h = x^h - \widehat{x}^h \tag{4}$$

The main task of the residual compression part is to construct a residual compression network, complete the probability distribution estimation and entropy encoding of r^h. This study uses a mixed logic model to fit the probability distribution of residuals, as shown in Figure 3.

In Figure 3, different parameter prediction sub networks are designed in the mixed logic model to complete the estimation of entropy parameters. Each prediction sub network is composed of 7×7's convolutional layer and Leaky ReLU function. The probability distribution $p_\theta\left(r^h\middle|u^h,C_{r^h}\right)$ of r^h is estimated and calculated using equation (5).

$$\begin{aligned} &p_\theta\left(r^h\middle|u^h,C_{r^h}\right) \\ &=\sum_{k=1}^{K}\pi_i^k\left[S\left(\frac{r_i^+-\mu_i^k}{\sigma_i^k}\right)-S\left(\frac{r_i^--\mu_i^k}{\sigma_i^k}\right)\right] \end{aligned} \tag{5}$$

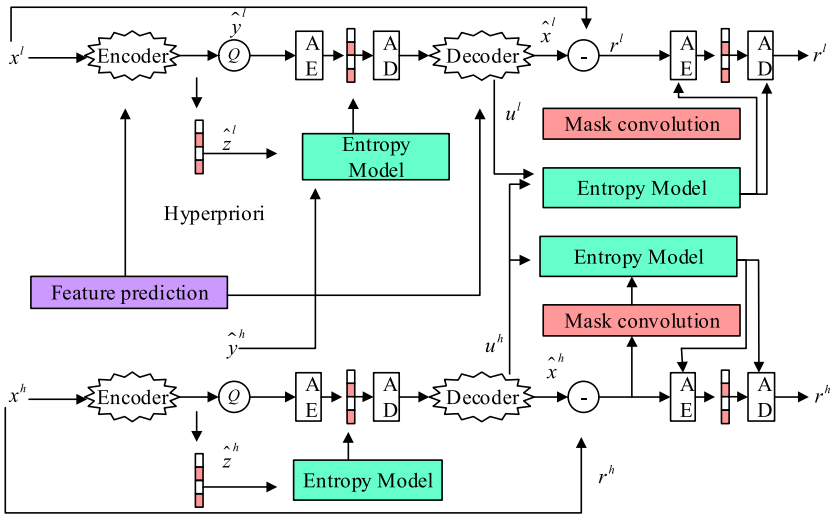

FIGURE 1. Schematic diagram of the two-stream compression model structure.

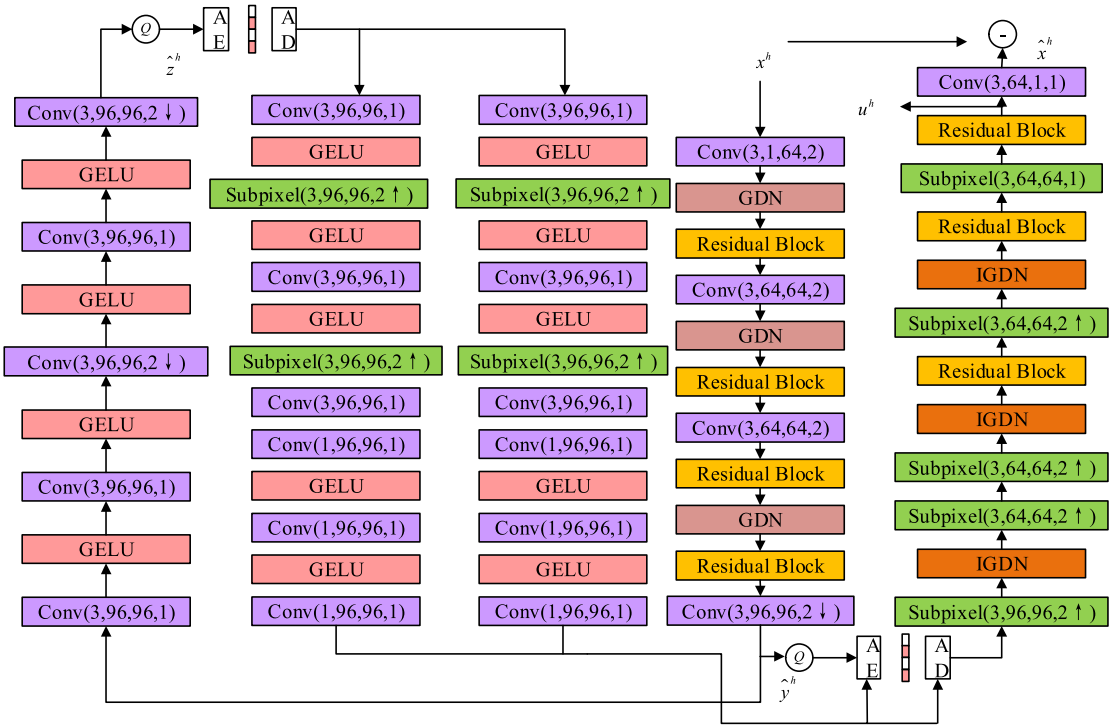

FIGURE 2. Compression model structure of the sub-graph module with a height of 8 bit depth.

In equation (5), C_{r^h} represents the contextual feature of r^h, which is extracted using mask convolution. π represents mixed weights. K represents the mixed quantity. k represents the logical distribution index. S represents the sigmoid function. r_i^+ and r_i^- represent r_i floating up and down by 0.5, respectively. Due to the use of a larger convolution kernel of 7×7 in the designed mixed logic model, the increase in the convolution kernel leads to an increase in the receptive field of the mixed logic model, which can further capture global information and improve the stability of feature extraction. However, the computational cost and over-fitting risk of the model increase, the model overly focuses on local details of the data, and the model's generalization decreases [17], [18]. In comparison, this study introduces the weighted moving average (WMA) method to average the model parameters, increase the robustness of the model, and reduce

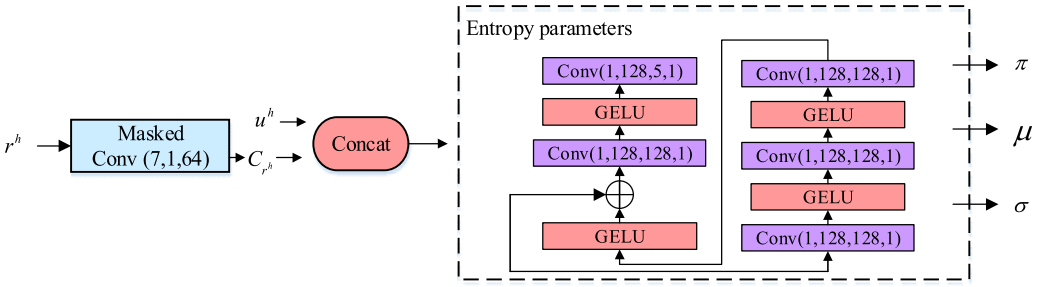

FIGURE 3. Flow of mixed logic model workflow.

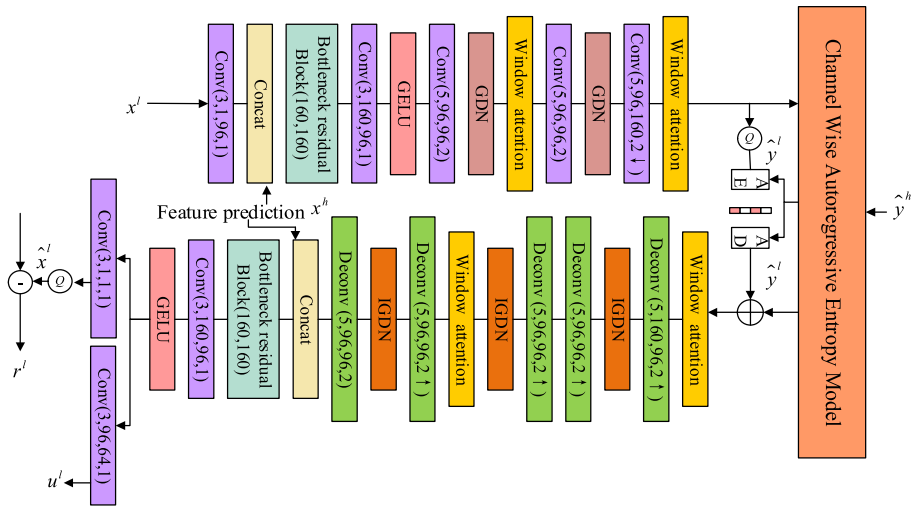

FIGURE 4. Compression model structure for the low 8b-DSG module.

over-fitting [19]. The recursive equation of WMA is equation (6).

$$v_t = \beta v_{t-1} + (1-\beta)\,\vartheta \tag{6}$$

In equation (6), v represents the time series of the given variable. t represents the timestamp. β represents a hyper-parameter between 0 and 1. ϑ represents the observed value of the current iteration.

B. DESIGN OF LOW 8B-DSG COMPRESSION NETWORK BASED ON LOSSY PLUS RESIDUAL

The low 8-bit deep sub-graph (8b-DSG) compression network is still based on a lossless and residual compression model, mainly using swapping modules and entropy models. The transformation module extracts and learns higher-level features by transforming data representations. This study uses a transformation module to convert high-dimensional pixel domain data into low dimensional feature domains, removing redundant information and noise from input data, facilitating the estimation of probability distribution, and reducing the compression rate of entropy coding. The lossy compression network model for low 8b-DSGs is Figure 4.

In Figure 4, the overall structure of the lossy compression network is still based on a hyper-priori model. However, due to the higher BR required for the low 8b-DSG x^l, x^l's compression network adopts a window attention mechanism to enhance the transformation module. After introducing the window attention mechanism, the model can focus on information from different regions at different time steps through parameter sharing, enhancing compression performance. The entropy model in the lossy compression network of the x^h sub-graph has added a channel auto-regressive model, forming the channel wise auto-regressive entropy model (CWAE).

In addition, this study adds an information exchange module between x^h and x^l compressed networks. One is that the entropy model of hidden feature $\widehat{y}^l$ in x^l integrates the hidden feature $\widehat{y}^h$ of sub-graph x^h. The second is to integrate the u^h of the x^h sub-graph in the residual entropy model. In the simultaneous transformation module, a feature prediction model is used to extract feature information from the x^h-compression network. The structural principle of feature prediction is Figure 5.

In Figure 5, the principle of the feature prediction model is similar to that of the hierarchical context extractor, which

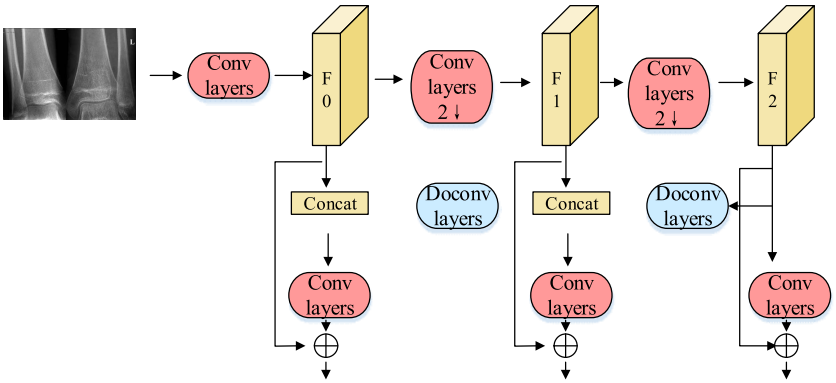

FIGURE 5. The structural principle of feature prediction.

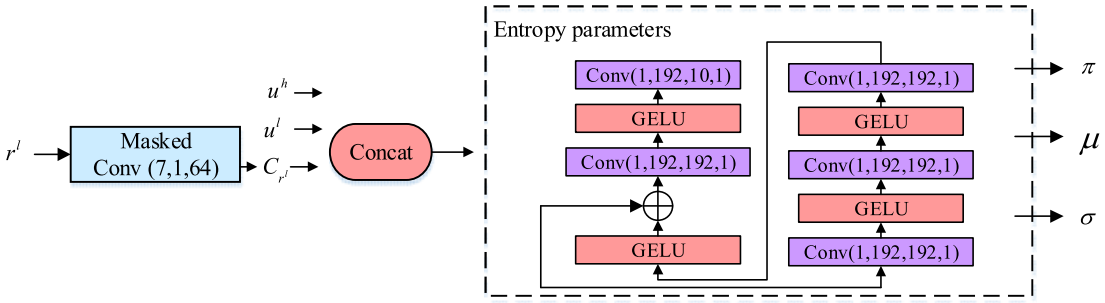

FIGURE 6. Mixed logic model structure for low 8b-DSGs.

uses a hierarchical approach to learn information at different scales [20]. This hierarchical extractor includes a downsampling path, an upsampling path, and a skip connection module. The downsampling path gradually expands the receptive field through a series of convolutional and pooling layers, and calculates feature maps at multiple scales. The calculation of downsampling feature F^n is equation (7).

$$F^n = f_{extract}\left(x^h\right), n = 0, 1, 2 \tag{7}$$

In equation (7), n represents the scaling step size. The upsampling path samples F^{n+1} through the deconvolution layer, achieving the combination of local information in the low-level feature map and global information in the high-level feature map. Combined with information $\widetilde{F}^n$, the calculation is shown in equation (8).

$$\widetilde{F}^n = concat\left(F^n, f_{upsample}\left(F^{n+1}\right)\right), n = 0, 1 \tag{8}$$

Finally, complementary information is added to F^n to generate the final prediction information $\overline{C}^n$, as calculated in equation (9).

$$\overline{C}^n = F^n + f_{complement}\left(\widetilde{F}^n\right), n = 0, 1, 2 \tag{9}$$

The designed feature prediction model only outputs the original scale feature map, and then completes feature fusion with x^l through convolution, residual operation. The decoding features of the decoder are fused with the features of x^h in the same way, and finally, two convolution operations are used to obtain the lossy reconstruction $\widehat{x}^l$ of x^l and the corresponding feature u^l. The CWAE module can improve the accuracy of entropy model estimation of $\widehat{y}^l$ probability distribution. The calculation process of estimating probability distribution $p_{\theta^k}\left(\widehat{y}^l \middle| \widehat{z}^l\right)$ and BR $R_{\widehat{y}^l,\widehat{z}^l}$ is consistent with the calculation method of high 8-bit deep sub-graph. The residual compression part of the low 8b-DSG compression network also adopts a mixed logic model, and the structural composition is Figure 6.

The calculation expression of residual r^l is equation (10).

$$r^l = x^l - \widehat{x}^l \tag{10}$$

The input information of the mixed logic model includes residual features r^l and r^h of x^l and x^h, as well as contextual features of r^l. Compared to the mixed logic model of high 8b-DSGs, the input information of low 8b-DSG increases. Therefore, the number of feature channels increased from 128 to 192. The number of mixed logic models used for high and low 8b-DSG is 5 and 10, respectively. Combining high and low 8b-DSG compression networks yields end-to-end DSLC-Net. The loss function calculation of DSLC-Net is equation (11).

$$L = R_{\widehat{y}^h,\widehat{z}^h} + R_{\widehat{y}^l,\widehat{z}^l} + R_{r^h} + R_{r^l} + \lambda \cdot (\alpha \cdot D_h \cdot D_l) \tag{11}$$

In equation (11), λ represents the trade-off parameter. R_{r^h} and R_{r^l}, D_h and D_l represent the residual BR

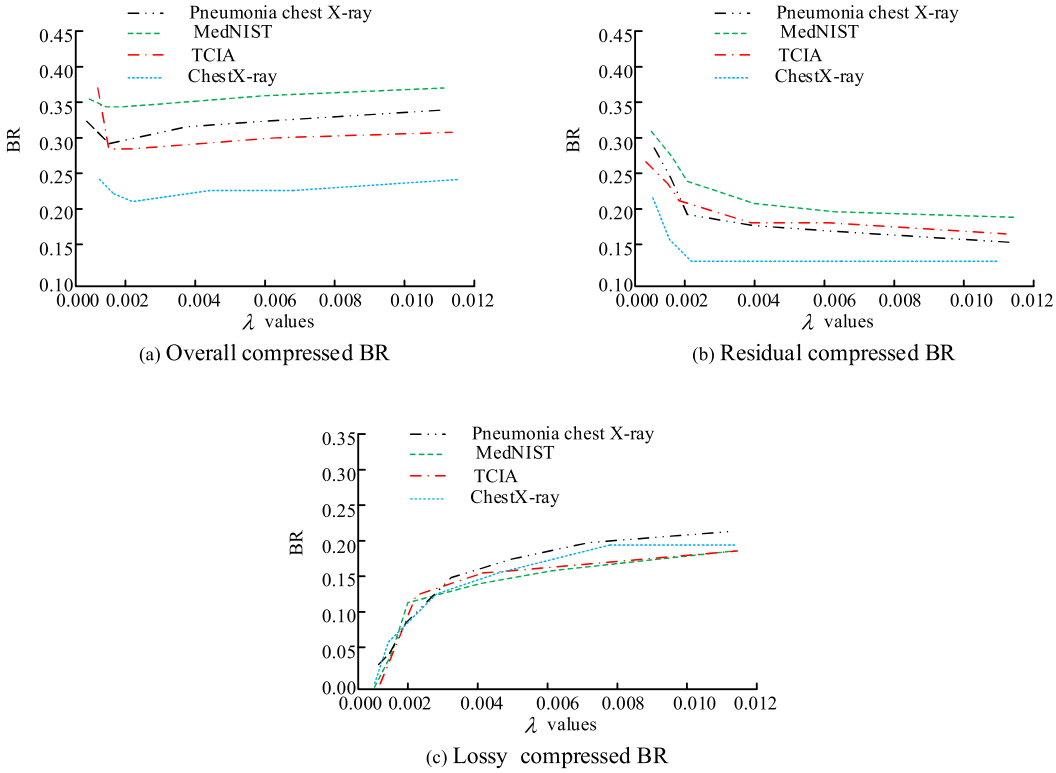

(a) Overall compressed BR

(b) Residual compressed BR

(c) Lossy compressed BR

FIGURE 7. The impact of different trade-off parameters on BR.

and distortion term of high and low 8b-DSG, respectively. α represents the control parameter of the distortion term. The calculation process of the distortion term is equation (12).

$$\begin{cases} D_h = \left(x^h - \widehat{x}^h\right)^2 \\ D_l = \left(x^l - \widehat{x}^l\right)^2 \end{cases} \tag{12}$$

In the dual stream compression network, the autoregressive model acceleration algorithm used in this study is PixelCNN. PixelCNN generates new images by learning the probability distribution between image pixels, as shown in equation (13).

$$p_\theta(x) = \prod_{i=1}^{n^2} p\left(x_i \left| x_1, \ldots, x_{i-1}\right.\right) \tag{13}$$

In equation (13), x_i represents the pixel value. $p_\theta(x)$ represents the product of the conditional distributions of different pixels.

IV. PERFORMANCE TESTING AND APPLICATION ANALYSIS OF A DUAL STREAM MODEL FOR NON-DESTRUCTIVE COMPRESSION OF BONE X-RAY IMAGES

To test the performance and clinical diagnostic application of the designed lossless compression dual stream model, this study constructed a performance testing experiment for the model and analyzed and discussed the results.

A. PERFORMANCE TESTING OF LOSSLESS COMPRESSION DUAL STREAM MODEL

The hardware environment used in the experiment is Windows 10, with a processor of Intel(R) Core(TM) i5-8500 CPU @3.00GHz, GPU of GeForce GTX1080Ti*2, and memory of 64G. The lossless compression framework in the software environment is implemented based on PyTorch 1.4, and the programming language is Python 3.6. Using the medical field HDR imaging dataset as the experimental dataset, the dataset is divided into training and testing sets in an 8:2 ratio according to the experimental needs. There are four datasets. A dataset containing chest X-rays of pneumonia, including 5,863 JPEG format X-ray images. The MedNIST dataset includes medical images of X-rays, CT, and MRI. The TCIA dataset contains medical image data of common tumors. The ChestX-ray dataset contains 112,120 X-ray images from frontal views.

The experiment selected a Joint Photographic Experts Group 2000 (JPEG2000)-based image compression standard using wavelet transform, a mixed compression model combining huffman coding (HC) and Lempel-Ziv-Welch (LZW) with rearranged information [6], and a residual encoding lossless compression framework based on Bilateral Context Modeling-based Network (BCM-Net) [7]. DSLC-Net has

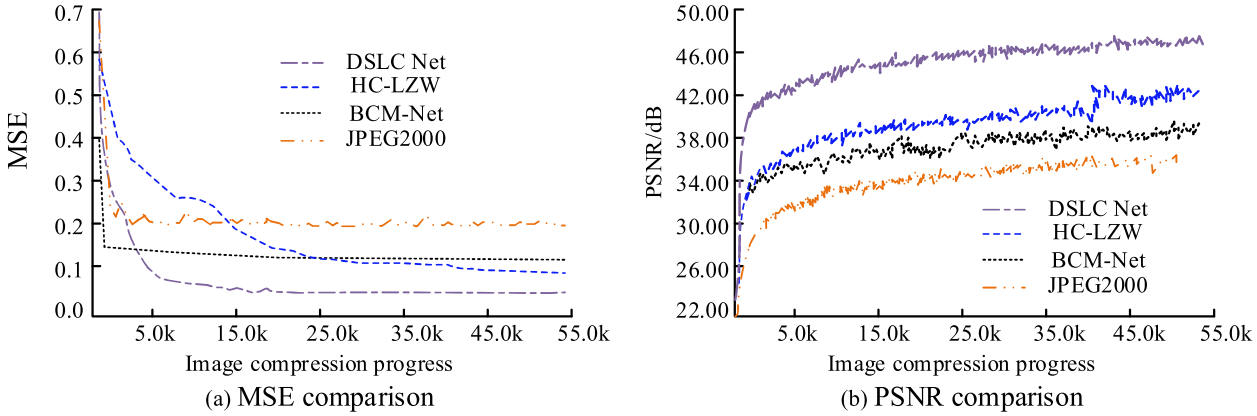

FIGURE 8. MSE and PSNR of different models.

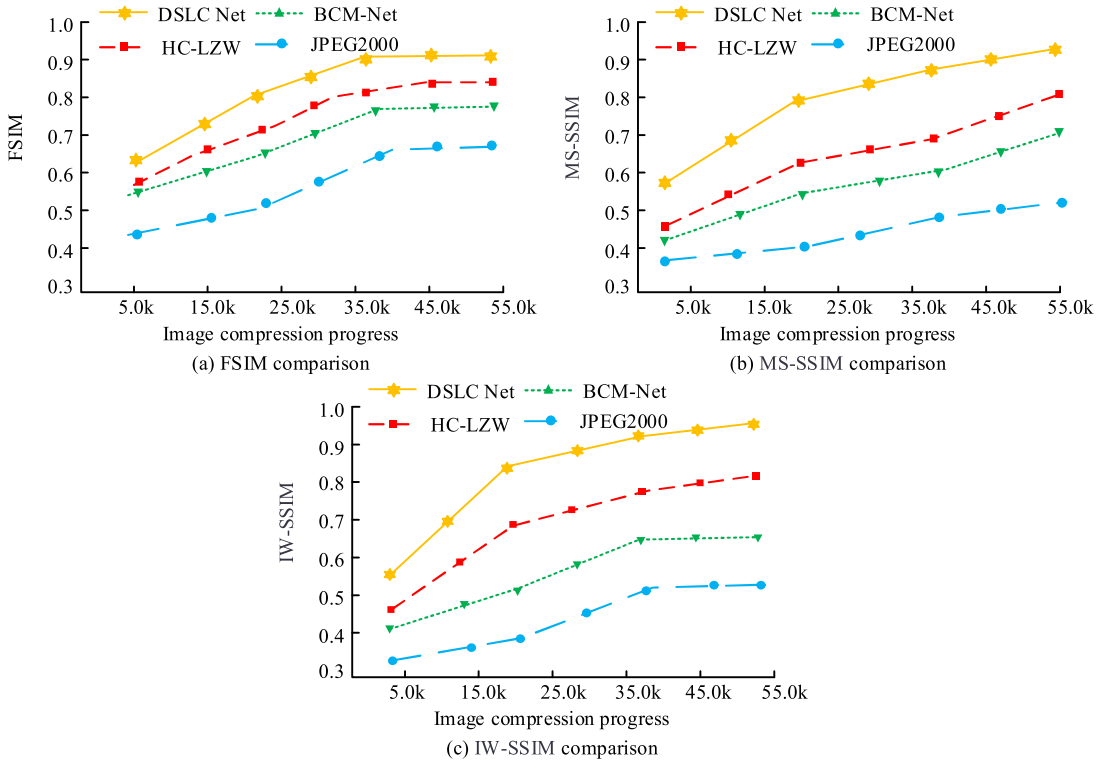

FIGURE 9. Comparison of SSIM of different models.

the best compression performance. The impact of different trade-off parameters on BR is Figure 7.

In Figure 7(a), on different datasets, as λ increases, the BR of DSLC-Net shows a trend of first decreasing and then increasing. When $\lambda = 0.001$ is present, the BR value of DSLC-Net is the smallest and reaches its optimal value. In Figures 7(b) and 7(c), as λ increases, the compression residual BR value of the model gradually decreases, the BR value of lossy encoding gradually increases, and the proportion of BR decreases. Based on the variation pattern of the total BR value in Figure 7(a), increasing the BR of lossy encoding does not improve the performance of the model. Table 1 shows the comparison results between CR and BR.

TABLE 1. Comparison of CR and BR for different compression models.

Model	Index	Pneumonia chest X-ray	MedNIST	TCIA	ChestX-ray
DSLC-Net	BR	0.297	0.348	0.275	0.204
	CR	0.942	0.946	0.904	0.931
JPEG2000	BR	0.446	0.597	0.603	0.513
	CR	0.698	0.703	0.716	0.679
HC-LZW	BR	0.467	0.493	0.408	0.413
	CR	0.716	0739	0.748	0.794
BCM-Net	BR	0.526	0.487	0.564	0.414
	CR	0.806	0.794	0.816	0.826

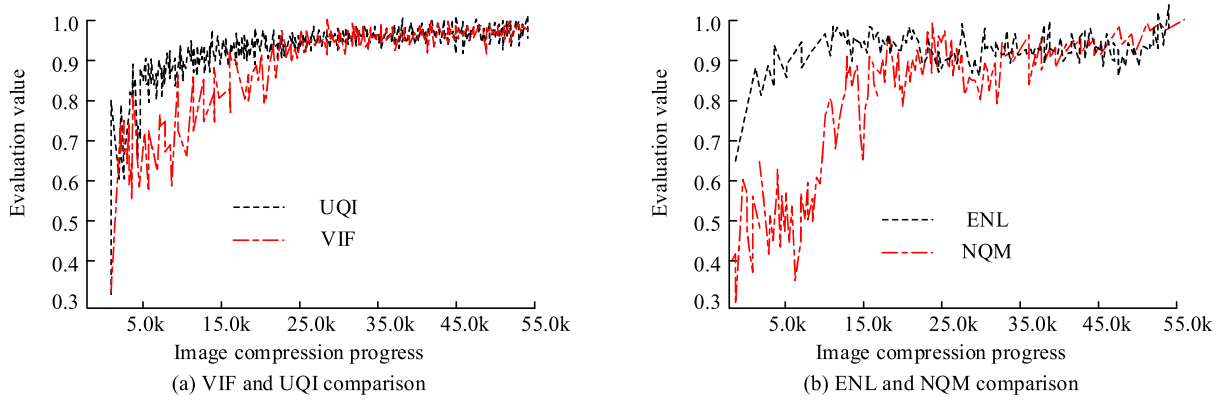

FIGURE 10. Quality evaluation of compressed images.

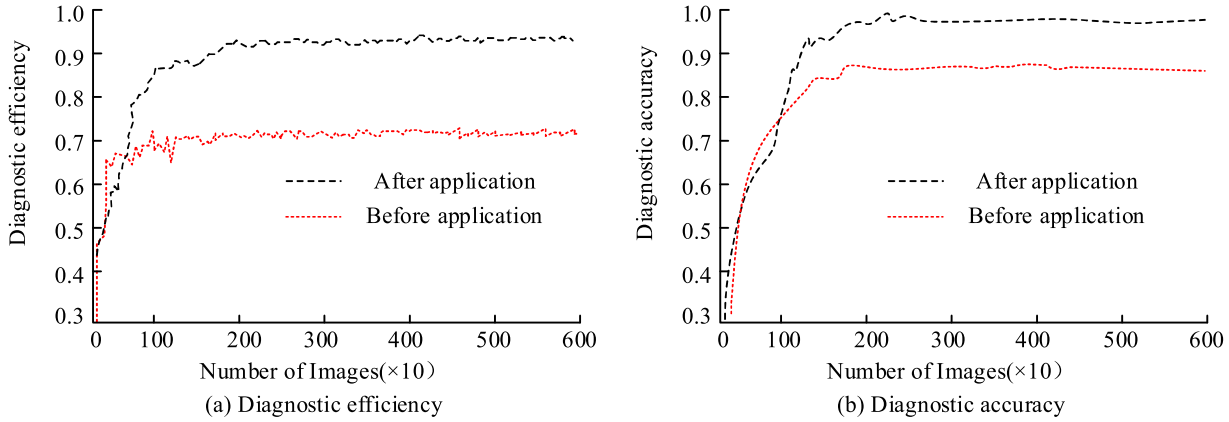

FIGURE 11. Diagnostic impact of lossless compression on osteoporosis.

In Table 1, the lowest BR for DSLC-Net is 0.204, and the highest BR is 0.348. Compared to JPEG2000, the highest reduction in BR reached 66.16%. Compared to the HC-LZW model, the highest reduction in BR reached 58.62%. Compared to BCM-Net, BR experienced a maximum decrease of 63.82%. DSLC-Net has a high degree of compression for image data and achieved good BR performance. Meanwhile, the CR value level of DSLC-Net is the highest, all above the 0.90 level, with a maximum value of 0.946. The experimental results of mean squared error (MSE) and peak signal-to-noise ratio (PSNR) are shown in Figure 8.

In Figure 8(a), the MSE of different compression models decreases continuously as the image compression process progresses, and the MSE of DSLC-Net converges to the minimum value of 0.07. The MSE values of the other three models are all above the 0.1 value level, with the highest MSE value of 0.24 for JPEG2000. In Figure 8(b), the corresponding DSLC-Net has the highest PSNR value, which rapidly rises above 40 dB during the initial compression stage. This indicates that the similarity between the original image and the compressed image is high, the image quality is good, and the distortion is within an acceptable range. In contrast, the PSNR value of JPEG2000 converges to around 34 dB, which is 9.09 dB lower than the PSNR value of DSLC-Net.

B. DIAGNOSIS AND ANALYSIS OF OSTEOPOROSIS BASED ON LOSSLESS COMPRESSION DUAL FLOW MODEL

From 2023 to 2024, medical imaging data of osteoporosis patients who underwent X-ray examination at a public tertiary hospital in China were collected and processed into images of 256 × 256 size. The structural similarity index (SSIM) results of X-ray image compression processing using different models are shown in Figure 9.

In Figure 9(a), the feature similarity index (FSIM) curve of DSLC-Net is the highest, with a value of 0.9. The image after lossless compression is relatively similar in the feature space. In Figure 9(b), DSLC-Net still outperforms the other three models in the multi-scale structural similarity index (MS-SSIM), with improvements of 0.45, 0.20, and 0.11 compared to JPEG2000, HC-LZW, and BCM-Net, respectively. Therefore, the compression processing effect of DSLC-Net on images is the best at different spatial scales. In Figure 9(c), DSLC-Net has a significant advantage with an information content weighted SSIM (IW-SSIM) value of

0.94. This network can effectively balance the importance of different parts of the image and improve the quality of image compression. The results of visual information fidelity (VIF), equivalent number of views (ENL), universal quality index (UQI), and noise quality measure (NQM) before and after compression of X-ray images are shown in Figure 10.

In Figure 10(a), the compressed image performs well on UQI and VIF, and the results of both evaluation indicators reach a value level of 0.9 in the later stage of compression. The overall visual quality and fidelity of compressed images are good, and the subjective visual effect is better. In Figure 10(b), the lossless compression network achieved high values on ENL and NQM, with ENL reaching 0.93 and NQM reaching 0.94. Overall, DSLC-Net has strong noise resistance and its compressed visual performance is not significantly affected. The compressed X-ray image data is used for remote diagnosis of osteoporosis, and the comparison between diagnostic efficiency and accuracy is Figure 11.

In Figure 11, after applying the DSLC-Net lossless compression network, the clinical diagnostic efficiency of osteoporosis patients improved by 0.22 and the diagnostic accuracy improved by 0.14. Lossless compression technology has improved the diagnostic performance of remote treatment processes. The compressed image has high fidelity, reducing the interference of image compression on disease diagnosis during remote diagnosis.

V. CONCLUSION

X-ray imaging plays an important clinical diagnostic role in bone density measurement, osteoporosis detection, and prevention and treatment. To improve the lossless compression quality of images, this study designed a lossless compression dual stream network suitable for X-ray HDR images based on DL technology. The experiment showed that when the balance parameter was set to 0.001, the BR of DSLC-Net was optimal. Compared to other models, the lowest BR of DSLC-Net was 0.204, and compared to JPEG2000, the highest BR reduction was 66.16%. For different datasets, the CR values of DSLC-Net were all above the 0.90 level, and the PSNR values of the images were higher than 40 dB, indicating a high degree of similarity before and after compression. DSLC-Net has achieved a relatively good evaluation level in FSIM, MS-SSIM, and IW-SSIM indicators. The four evaluation indicators of VIF, ENL, UQI, and NQM have verified the visual authenticity of the images, ensuring the diagnostic efficiency and accuracy of osteoporosis. The performance of the lossless compression network designed in this study has been significantly improved, which is helpful for the transmission, storage, and clinical diagnosis of medical image data, and has important application significance in X-ray diagnosis of osteoporosis. Future research can explore more lossless compression frameworks to accelerate the progress of lossless compression.

REFERENCES

[1] J. A. Kanis, E. V. McCloskey, N. C. Harvey, C. Cooper, R. Rizzoli, B. Dawson-Hughes, S. Maggi, and J.-Y. Reginster, "The need to distinguish intervention thresholds and diagnostic thresholds in the management of osteoporosis," *Osteoporosis Int.*, vol. 34, no. 1, pp. 1–9, Jan. 2023.

[2] E. Shevroja, J.-Y. Reginster, O. Lamy, N. Al-Daghri, M. Chandran, A.-L. Demoux-Baiada, L. Kohlmeier, M.-P. Lecart, D. Messina, B. M. Camargos, J. Payer, S. Tuzun, N. Veronese, C. Cooper, E. V. McCloskey, and N. C. Harvey, "Update on the clinical use of trabecular bone score (TBS) in the management of osteoporosis: Results of an expert group meeting organized by the European society for clinical and economic aspects of osteoporosis, osteoarthritis and musculoskeletal diseases (ESCEO), and the international osteoporosis foundation (IOF) under the auspices of WHO collaborating center for epidemiology of musculoskeletal health and aging," *Osteoporosis Int.*, vol. 34, no. 9, pp. 1501–1529, Sep. 2023.

[3] M. Chandran, K. Brind'Amour, S. Fujiwara, Y.-C. Ha, H. Tang, J.-S. Hwang, J. Tinker, and J. A. Eisman, "Prevalence of osteoporosis and incidence of related fractures in developed economies in the Asia Pacific region: A systematic review," *Osteoporosis Int.*, vol. 34, no. 6, pp. 1037–1053, Jun. 2023.

[4] W. Lin, Y. Zhang, W. Dai, H. Liu, J. See, and H. Xiong, "Scene graph lossless compression with adaptive prediction for objects and relations," *ACM Trans. Multimedia Comput., Commun., Appl.*, vol. 20, no. 7, pp. 1–23, Jul. 2024.

[5] A. Altamimi and B. Ben Youssef, "Lossless and near-lossless compression algorithms for remotely sensed hyperspectral images," *Entropy*, vol. 26, no. 4, pp. 316–351, Apr. 2024.

[6] H. Mohammadi, A. Ghaderzadeh, and A. Sheikh Ahmadi, "A novel hybrid medical data compression using Huffman coding and LZW in IoT," *IETE J. Res.*, vol. 69, no. 11, pp. 7831–7845, Nov. 2023.

[7] X. Liu, M. Wang, S. Wang, and S. Kwong, "Bilateral context modeling for residual coding in lossless 3D medical image compression," *IEEE Trans. Image Process.*, vol. 33, no. 5, pp. 2502–2513, Mar. 2024.

[8] A. Daoui, H. Mao, M. Yamni, Q. Li, O. Alfarraj, and A. A. A. El-Latif, "Novel integer shmaliy transform and new multiparametric piecewise linear chaotic map for joint lossless compression and encryption of medical images in IoMTs," *Mathematics*, vol. 11, no. 16, pp. 3619–3646, Aug. 2023.

[9] S. Boopathiraja, P. Kalavathi, S. Deoghare, and V. B. S. Prasath, "Near lossless compression for 3D radiological images using optimal multilinear singular value decomposition (3D-VOI-OMLSVD)," *J. Digit. Imag.*, vol. 36, no. 1, pp. 259–275, Aug. 2022.

[10] I. Jumakulyyev and T. Schultz, "Combining image space and q-space PDEs for lossless compression of diffusion MR images," *J. Math. Imag. Vis.*, vol. 65, no. 4, pp. 644–656, Aug. 2023.

[11] J. Jiang, X. Xie, X. Yu, Z. You, and Q. Hu, "RCA-PixelCNN: Residual causal attention PixelCNN for pulsar candidate image lossless compression," *Appl. Sci.*, vol. 13, no. 19, pp. 10941–10956, Oct. 2023.

[12] P. Yadav, A. K. Pandey, J. Chaudhary, P. D. Sharma, J. Jaleel, V. Baghel, C. Patel, and R. Kumar, "Near-lossless compression of Tc-99 m DMSA scan images using discrete cosine transformation," *Indian J. Nucl. Med.*, vol. 38, no. 3, pp. 231–238, 2023.

[13] X. Liu, P. An, Y. Chen, and X. Huang, "An improved lossless image compression algorithm based on Huffman coding," *Multimedia Tools Appl.*, vol. 81, no. 4, pp. 4781–4795, Feb. 2022.

[14] V. P. Reddy, R. M. Prasad, P. Udayaraju, B. H. Naik, and C. Raja, "Efficient medical image security and transmission using modified LZW compression and ECDH-AES for telemedicine applications," *Soft Comput.*, vol. 27, no. 13, pp. 9151–9168, Jul. 2023.

[15] A. Basit, W. T. Toor, M. Saadi, N. Maroof, S. A. Khan, and S. A. Otaibi, "Reversible encryption and lossless data hiding for medical imaging aiding smart health care," *Cluster Comput.*, vol. 26, no. 5, pp. 2977–2991, Oct. 2023.

[16] P. Preethi and H. R. Mamatha, "Region-based convolutional neural network for segmenting text in epigraphical images," *Artif. Intell. Appl.*, vol. 1, no. 2, pp. 119–127, Sep. 2022.

[17] S. Ahmadzadeh, "Study of energy-efficient biomedical data compression methods in the wireless body area networks (WBANs) and remote healthcare networks," *Int. J. Wireless Inf. Netw.*, vol. 30, no. 3, pp. 252–269, Sep. 2023.

[18] O. P. Singh, K. N. Singh, N. Baranwal, A. K. Agrawal, A. K. Singh, and H. Zhou, "HIDEmarks: Hiding multiple marks for robust medical data sharing using IWT-LSB," *Multimedia Tools Appl.*, vol. 83, no. 8, pp. 24919–24937, Aug. 2023.
[19] L. Xiao, B. Zou, and X. Kui, "A secure lossless redundancy elimination scheme with semantic awareness for cloud-assisted health systems," *IEEE Syst. J.*, vol. 17, no. 3, pp. 4615–4626, Mar. 2023.
[20] A. Afnan, F. Ullah, Y. Yaseen, J. Lee, S. Jamil, and O.-J. Kwon, "Subjective assessment of objective image quality metrics range guaranteeing visually lossless compression," *Sensors*, vol. 23, no. 3, pp. 1297–1313, Jan. 2023.

CHAO JIANG received the bachelor's degree from Jiangxi University of Traditional Chinese Medicine, in June 2014.

He worked clinically with the Orthopedics Department, Yushan County Traditional Chinese Medicine Hospital, Shangrao, Jiangxi, from July 2014 to September 2016. He worked with Haining Fuchun Orthopedic Hospital, Jiaxing, Zhejiang, from October 2016 to March 2023, mainly engaged in trauma orthopedics and spinal surgery. He has been with the Orthopedics and Traumatology Department, Changshan County Hospital of Traditional Chinese Medicine, Quzhou, Zhejiang, since April 2023. His research interests include the clinical diagnosis of osteoporosis, the application of traditional Chinese medicine in the treatment of osteoporosis, and the clinical application of traditional Chinese medicine technology in grassroots hospitals.

YUQI CHENG received the degree from Quzhou Health School, in 1992, and the bachelor's degree in clinical medicine from Hangzhou Normal University, in 2011.

He is currently the Chief Physician, the Director of the Orthopedics and Traumatology Department, Changshan County Hospital of Traditional Chinese Medicine, and a Renowned Physician in Changshan County. He has undergone multiple advanced studies in the Department of Orthopedics, Shanghai Jiao Tong University Affiliated Sixth People's Hospital, Zhejiang University School of Medicine Affiliated Second Hospital, and Zhejiang Provincial People's Hospital. He has been working in orthopedics for more than 20 years and have been dedicated to research on the diagnosis and treatment of osteoporotic fractures for a long time. Proficient in: conservative and surgical treatment of limb fractures, replantation of severed limbs (fingers and toes), and flap repair surgery for soft tissue defects; conservative and surgical treatment for spinal injuries, infections, and degenerative diseases; joint replacement surgery and arthroscopic surgery for joint lesions; diagnosis and treatment of bone and soft tissue tumors. He is a member of the Orthopedics Branch of Zhejiang Social Medical Association, the Orthopedics and Trauma Specialized Committee of Quzhou Society of Traditional Chinese and Western Medicine, and the Sports Medicine Branch of Quzhou Medical Association. He is the Director of Quzhou Integrated Traditional Chinese and Western Medicine Society.

BAOSHENG CHENG received the degree major in traditional Chinese medicine orthopedics and the bachelor's degree in adult medicine from Jiangxi University of Traditional Chinese Medicine, in July 2010 and 2016, respectively.

Since 2010, he has been engaged in clinical work in orthopedics and traumatology, with more than 13 years of clinical experience in orthopedics. He is currently working with the Orthopedics and Traumatology Department, Changshan County Hospital of Traditional Chinese Medicine, Quzhou, Zhejiang. His research interests include the causal relationships of sports medicine in work and life, diagnosis and treatment standards for elderly osteoporotic fractures, and observation of the early therapeutic effect of traditional Chinese medicine's external application technology on soft tissue swelling.